

Spatial dependence of high energy electrons and their radiations in pulsar wind nebulae

Fang-Wu Lu^{1,2}, Quan-Gui Gao^{1,2} and Li Zhang¹

¹ Department of Astronomy, Key Laboratory of Astroparticle Physics of Yunnan Province, Yunnan University, Kunming 650091, China; lizhang@ynu.edu.cn

² Department of Physics, Yuxi Normal University, Yuxi 653100, China

Received 2015 September 7; accepted 2016 February 29

Abstract We investigate the spatial dependence of high energy electrons and their radiations in pulsar wind nebulae (PWNe). By assuming a time-dependent broken power-law injection and spatial dependence of convection velocity, magnetic field strength and diffusion coefficient on the radial distance of an expanding system, we numerically solve the Fokker-Planck transport equation including convection, diffusion, adiabatic loss and radiative loss in spherical coordinates, and investigate the effects of magnetic field, PWN age, maximum energy of electrons, and diffusion coefficient on electron spectra and non-thermal photon emissions. Our results indicate that (1) electron spectra and the corresponding photon spectra are a function of radial distance r of the expanding system; (2) for a given expansion velocity, the increase of the PWN age causes a slower decrease of the convection velocity ($V \propto r^{-\beta}$) and a more rapid decrease of the magnetic field strength ($B \propto r^{-1+\beta}$), but a more rapid increase of the diffusion coefficient ($\kappa \propto r^{1-\beta}$) because the index β decreases with the PWN age; and (3) the lower energy part of the electron spectra is dominated by convection and adiabatic loss, but the higher energy part is dominated by the competition between synchrotron loss and diffusion, and such a competition is a function of radial distance. Therefore the diffusion effect has an important role in the evolution of electron spectra as well as non-thermal photon spectra in a PWN.

Key words: diffusion — ISM: supernova remnants — pulsars: general — radiation mechanisms: non-thermal

1 INTRODUCTION

Pulsar wind nebulae (PWNe) are generally believed to be accelerators which can accelerate particles to extreme relativistic energy. Indirect evidence of particle acceleration in a PWN can come from the multiband observations of photon emissions from the PWN. In fact, if the non-thermal emissions at radio - X-ray and GeV - TeV bands are produced by synchrotron radiation and inverse Compton scattering of relativistic electrons respectively, then electron energies in a PWN can range from ~ 1 GeV to ~ 1 PeV. Up to now, about 70 PWNe that emit X-ray photons and about 30 PWNe that emit TeV photons (see a review of Kargaltsev et al. 2014) have been detected; all of these observations provide basic information for us to study the acceleration of particles and the radiation processes in PWNe.

Various models have been proposed to explain multiband photon emissions from PWNe. In these models, PWNe are maintained solely by the pulsar rotational power and the relativistic particles come directly from the pulsar magnetosphere (Rees & Gunn 1974; Kennel & Coroniti

1984). At present, popular models are preferred to leptonic ones. The multiband observations of photon emissions from the PWN indicated that the electron spectrum can be divided into two distinct components (Weiler & Panagia 1978; Gaensler & Slane 2006; Vorster et al. 2013): a low-energy component producing the radio synchrotron and GeV inverse Compton emission and a high-energy component producing the X-ray synchrotron and TeV inverse Compton emission. Furthermore, Atoyan & Aharonian (1996) assumed that the two components are the radio electron component (produced inside the light cylinder of the pulsar) and the wind electron component (produced at the shock radius by a Fermi-type process). Therefore, the particle evolution models often use a broken power-law to describe the spectrum of the injected relativistic electrons with different indices and some break energy (e.g., Venter & de Jager 2006; Zhang et al. 2008; Tanaka & Takahara 2010; Martín et al. 2012). Non-thermal photons from radio to TeV bands for a given PWN are produced by the synchrotron radiation and the inverse Compton scattering off various soft photons, i.e., synchrotron photons, cosmic microwave background (CMB), infrared (IR) photons and

starlight (e.g., Zhang et al. 2008; Tanaka & Takahara 2010; Li et al. 2010; Fang & Zhang 2010; Martín et al. 2012; Vorster et al. 2013; Torres et al. 2014; Zhu et al. 2015). In these models, a simplified time-dependent uniform injection in the whole nebula is assumed. However, some of the papers did not consider the effect of particle diffusion, and others considered the particle diffusion as the escape of the particles.

Recently, Vorster & Moraal (2013) (hereafter VM13) studied the effect of diffusion on the particle spectra in a PWN. In their model, a steady-state injection with a single power-law form is assumed, and the distribution of particles is described as the Fokker-Planck transport equation, which includes the processes of convection, diffusion, adiabatic loss and synchrotron loss. They numerically solved the time-dependent transport equation and concluded that diffusion can effectively reduce the amount of synchrotron loss and then can modify expected particle spectra.

Since the electron injection is time-dependent and has a broken power-law in a relativistic PWN model, in this paper, we revisit the effect of diffusion on the electron spectra in PWNe with a time-dependent broken power-law injection in the model of VM13. Moreover, we investigate non-thermal emissions in such a system. The organization of this paper is as follows. In Section 2, we describe the time-dependent particle injection and the transport equation related to particle evolutions. We describe the processes of non-thermal photon emission in Section 3, and we show calculation results in Section 4, including the effects of magnetic field, PWN age, maximum energy of electrons and diffusion on the particle spectral evolution and non-thermal photon spectra in a PWN. Finally, we give conclusions and discussions in Section 5.

2 TIME-DEPENDENT INJECTION AND EVOLUTION OF PARTICLES

2.1 Time-dependent Particle Injection

In order to understand the evolution of particles in a PWN, i.e., to solve the Fokker-Planck transport equation related to particle evolution, we must know the particle injection rate. Although there are at least three possible injection forms: a power-law (e.g., Gelfand et al. 2009), a broken power-law (e.g., Venter & de Jager 2006; Zhang et al. 2008), and a relativistic Maxwellian spectrum with a non-thermal power-law tail (e.g., Fang & Zhang 2010; Vorster et al. 2013), here we just use the second form, which has been widely adopted (e.g., Venter & de Jager 2006; Zhang et al. 2008; Tanaka & Takahara 2010; Martín et al. 2012; Torres et al. 2014; Zhu et al. 2015), i.e.,

$$Q(E_e, t) = \begin{cases} Q_0(t)(E_e/E_b)^{-\alpha_1} & \text{if } E_e < E_b, \\ Q_0(t)(E_e/E_b)^{-\alpha_2} & \text{if } E_e \geq E_b, \end{cases} \quad (1)$$

where $Q_0(t)$ is the normalization coefficient, α_1 and α_2 are the power-law indices at the low and high energy ranges of the injection spectrum, respectively, and E_b is a break energy.

For a rotation-powered pulsar, the evolution of the spin-down power $L(t)$ is given by

$$L(t) = L_0 \left[1 + \frac{(n-1)P_0^2 L_0 t}{4\pi^2 I} \right]^{-(n+1)/(n-1)}, \quad (2)$$

where L_0 is the spin-down power, P_0 is the pulsar period at the pulsar's birth, n is the braking index and assumed to be a constant, and I is the moment of inertia. After assuming the particle's total energy per unit time is some fraction of $L(t)$, i.e., $\int Q(E_e, t) E_e dE_e = (1-\eta)L(t)$, where η is the magnetic energy fraction of the spin-down power into particle luminosity (here we set $\eta \sim 0.03$ as a parameter, which is the same as that used in Torres et al. 2014), we can estimate the normalization coefficient $Q_0(t)$, which is

$$Q_0(t) = \frac{(1-\eta)L(t)}{E_b^2} \times \begin{cases} \frac{(2-\alpha_1)(2-\alpha_2)}{\alpha_1 - \alpha_2} & \alpha_2 > 2, \\ \left[\frac{1}{2-\alpha_1} + \log\left(\frac{E_{\max}}{E_b}\right) \right]^{-1} & \alpha_2 = 2. \end{cases} \quad (3)$$

2.2 Particle Evolution

A general transport equation describing a particle's convection and diffusion is called the Fokker-Planck equation (e.g., Parker 1965). In order to study the effect of diffusion on the particle spectra in PWNe, VM13 considered such a system with spherical symmetry (i.e., $\partial f/\partial\phi = 0 = \partial f/\partial\theta = 0$, where f is the distribution function) and without momentum diffusion (i.e., $D_p \partial f/\partial p = 0$, where D_p is the momentum diffusion coefficient) in spherical coordinates. For a system with an initial radius r_s , since the outer boundary of the nebula is expanding, VM13 transformed the system with an expanding outer boundary (the expanding system) to one with a static outer boundary (the static system) by using the transformation $r = \rho(r', t)r' + \varepsilon(r', t)$, where

$$\begin{aligned} \rho(r', t) &= \left[V_{\text{pwn}} \left(\frac{t-t_0}{r'_1 - r'_0} \right) \right] + 1 \\ \varepsilon(r', t) &= -V_{\text{pwn}} \left(\frac{t-t_0}{r'_1 - r'_0} \right) r'_0. \end{aligned} \quad (4)$$

V_{pwn} is the expansion velocity of the nebula, r is a coordinate in the expanding system, and r' is a coordinate in the static system with an inner boundary r'_0 and an outer boundary r'_1 , and t_0 is the time when expansion starts. Then they deduced the transport equation as follows:

$$\begin{aligned} \frac{\partial f'}{\partial t} &= \frac{\kappa}{\rho^2} \frac{\partial^2 f'}{\partial r'^2} \\ &+ \frac{1}{\rho} \left[\frac{2\kappa}{\rho r' + \varepsilon} + \frac{1}{\rho} \frac{\partial \kappa}{\partial r'} - V + \frac{\partial r}{\partial t} \right] \frac{\partial f'}{\partial r'} \\ &+ \left[\frac{2V}{3(\rho r' + \varepsilon)} + \frac{1}{3\rho} \frac{\partial V}{\partial r'} + zE \right] \frac{\partial f'}{\partial \ln E} \\ &+ 4zE f' + Q, \end{aligned} \quad (5)$$

where $f'(r', t) = f(\rho r' + \varepsilon, t) = f(r, t)$ is the distribution function in the expanding system, r' is the radial distance in units of r_S , t is the time in units of the light transition time r_S/c through the system, κ is the diffusion coefficient in units of $r_S c$, V is the convection velocity in units of c , $\partial r/\partial t = V_{\text{pwn}}(r' - r'_0)/(r'_1 - r'_0)$, E is the particle energy in units of a certain energy E_S (here we set $E_S = 1$ MeV), and Q is the source term given by Equation (1). In Equation (5), the quantity z is given by

$$z = \frac{4\sigma_T c}{3m_0 c^2} \frac{E_S}{m_0 c^2} (U_B + U_{\text{IC}}) \frac{r_S}{c}, \quad (6)$$

where σ_T is the Thomson scattering cross-section, $U_B = B^2/8\pi$ is the energy density of the magnetic field, U_{IC} is the energy density of the target photon fields, and m_0 is the rest mass of the particles. Here, the target photon fields include the synchrotron photons, the CMB, far IR (FIR), and starlight. Note that in our treatment of U_{IC} , the Klein-Nishina effects are included according to Moderski et al. (2005), that is $U_{\text{IC}} = \int_{\epsilon_0, \min}^{\epsilon_0, \max} f_{\text{KN}}(\tilde{b}) \epsilon_0 n(\epsilon_0) d\epsilon_0$, where $n(\epsilon_0)$ is the energy distribution of target photons, $\tilde{b} = (4E_S/m_0 c^2) E \epsilon_0$ and the function $f_{\text{KN}}(\tilde{b})$ is a factor in which the Klein-Nishina effects are included (see eqs. C5 and C3 of Moderski et al. 2005).

The specific expressions of V , κ and B are required before solving Equation (5). Following VM13, we assume that the convection velocity is

$$V = V_0 \left(\frac{r_0}{r} \right)^\beta. \quad (7)$$

Under the ideal magnetohydrodynamic (MHD) limit, the magnetic field B satisfies

$$B = B_0 \left(\frac{r_0}{r} \right)^{1-\beta}, \quad (8)$$

and the diffusion coefficient $\kappa(r, E)$ is expressed as

$$\kappa = \kappa_0 E \left(\frac{r_0}{r} \right)^{-1+\beta}, \quad (9)$$

where V_0 , B_0 and κ_0 are the convection velocity, magnetic field strength and diffusion coefficient at the inner boundary, respectively. Note that the index β is time-dependent and is defined by the convection velocity and expansion velocity in the system. In the outer boundary r_1 which is defined as $r_1 = \rho r'_1 + \varepsilon$, the convection velocity should be equal to the expansion velocity, $V_0(r_0/r_1)^\beta = V_{\text{pwn}}$, i.e.,

$$\beta = \frac{\ln V_0 - \ln V_{\text{pwn}}}{\ln[(\rho r'_1 + \varepsilon)/r'_0]}. \quad (10)$$

To solve the transport Equation (5), the Alternating Direction Implicit (ADI) method proposed by Douglas (1962) is used (for details on the discretization of Eq. (5) see Appendix A). In this method, the evolution time is chosen as the stepping parameter, and the initial condition is chosen as an empty system (see VM13). Meanwhile both inner and outer boundary conditions in the radial direction must be determined. In the inner boundary which is located

at the injection position r'_0 , the number of particles per energy interval that flow through the inner boundary must be equal to the total number of particles $Q(E_e, t)$. Following VM13, the inner boundary condition satisfies

$$C V_0 f' - \frac{\kappa_0}{\rho} \frac{\partial f'}{\partial r'} = \frac{1}{4\pi (r_S r'_0)^2} \frac{Q(E_e, t)}{4\pi (E_S E)^2}, \quad (11)$$

where C is the Compton-Getting coefficient and can be given by $C = -(1/3)(\partial \ln f' / \partial \ln E)$ in this case and V_0 is the convection velocity at r'_0 . To simulate particles escaping from the system, a free-escape $f'(r'_1, E) = 0$ should be chosen at the outer boundary. On the other hand, in the energy direction, particles should be able to escape from the energy space when they reach E_{min} , and the free-escape condition $f'(r', E_{\text{min}}) = 0$ should be imposed. For E_{max} , a free-escape boundary is also imposed.

Using the method described above, we can numerically calculate the distribution function $f(r, E, t)$ at a fixed radial distance r and time t . Then we can obtain corresponding particle density $dN/dEdV = N(r, E, t) = 4\pi E^2 f(r, E, t)$ which is defined as the number of electrons per unit volume in the energy interval $E + dE$, and the unit volume is defined as r_S^3 . Therefore, the number of electrons in the energy interval $E + dE$ can be given by

$$N_{\text{tot}}(E, t) = \int_{r_0}^{r_1} 4\pi r^2 N(r, E, t) dr, \quad (12)$$

where $r_1 = \rho r'_1 + \varepsilon$ with $r'_1 = 1$. In calculations of synchrotron and inverse Compton emission spectra, the electron intensity is usually used, which is defined as $J_e = (v_e/4\pi)N$, where v_e is the electron velocity.

Finally, to understand the effect diffusion has on the particle spectra, we give the expressions of diffusion timescale τ_{diff} , convection timescale τ_{con} , synchrotron cooling timescale τ_{syn} , inverse Compton cooling timescale τ_{IC} , and adiabatic loss timescale τ_{ad} as follows:

$$\tau_{\text{diff}} = \frac{r^2}{6\kappa} = \frac{r_0^2}{6\kappa_0} \frac{1}{E} \left(\frac{r}{r_0} \right)^{1+\beta}, \quad (13)$$

$$\tau_{\text{con}} = \int_{r_0}^r \frac{dr}{V(r)} = \frac{r_0}{(1+\beta)V_0} \left(\frac{r}{r_0} \right)^{1+\beta}, \quad (14)$$

$$\begin{aligned} \tau_{\text{syn}} &= \frac{3(m_0 c^2)^2}{4\sigma_T c U_B E_S E} \\ &= \frac{6\pi}{\sigma_T c} \frac{(m_0 c^2)^2}{B_0^2 E_S} \frac{1}{E} \left(\frac{r}{r_0} \right)^{2(1-\beta)}, \end{aligned} \quad (15)$$

$$\tau_{\text{IC}} = \frac{3(m_0 c^2)^2}{4\sigma_T c U_{\text{IC}} E_S E} = \frac{3}{4\sigma_T c} \frac{(m_0 c^2)^2}{U_{\text{IC}} E_S} \frac{1}{E}, \quad (16)$$

$$\tau_{\text{ad}} = \frac{3r^2}{\partial(r^2 V)/\partial r} = \frac{3r_0}{(2-\beta)V_0} \left(\frac{r}{r_0} \right)^{1+\beta}. \quad (17)$$

3 NON-THERMAL PHOTON EMISSION

When the relativistic particle distribution is determined, we can calculate the spectral evolution of non-thermal photons in a PWN. The radiation processes in our model consist of synchrotron radiation and inverse Compton scattering of the soft seed photons. For the synchrotron radiation, the emissivity is given by (e.g., Rybicki & Lightman 1979; Zhang & Fang 2007)

$$Q_{\text{syn}}(r, E_\gamma, t) = \frac{2\sqrt{3}e^3 B}{\hbar E_\gamma m_0 c^3} \int_0^{\pi/2} d\theta \sin^2 \theta \int_{E_{e,\text{min}}}^{E_{e,\text{max}}} dE_e J_e(r, E_e, t) R(E_\gamma/E_e), \quad (18)$$

where θ is the electron pitch angle, $E_c = 4.2 \times 10^6 \hbar B \gamma_e^2 \sin \theta$, B is the local magnetic field strength and

$$R(y) = y \int_y^\infty dz K_{5/3}(z) \quad (19)$$

with $y = E_\gamma/E_c$, here $K_{5/3}$ is a modified Bessel function of order $5/3$.

For the inverse Compton scattering, the emissivity is given by (e.g., Blumenthal & Gould 1970; Zhang & Fang 2007)

$$Q_{\text{Comp,j}}(r, E_\gamma, t) = 4\pi \int_0^\infty d\epsilon n_j(r, \epsilon) \int_{E_{e,\text{thresh}}}^{E_{e,\text{max}}} dE_e J_e(r, E_e, t) F_{\text{KN}}(\epsilon, E_\gamma, E_e), \quad (20)$$

where $E_{e,\text{thresh}} = (E_\gamma + [E_\gamma^2 + E_\gamma(m_0 c^2)^2/\epsilon]^{1/2})/2$ is the lowest energy, ϵ is the target photon energy and n_j is the distribution of the target photon fields. The energy distributions of the CMB, IR and starlight components are given by

$$n_j(\epsilon) = \frac{15U_j}{(\pi k T_j)^4} \frac{\epsilon^2}{\exp(\epsilon/kT_j) - 1}. \quad (21)$$

The distribution of the synchrotron radiation is given by (Atayan & Aharonian 1996)

$$n_{\text{syn}}(r, \epsilon, t) = \frac{1}{2c} \int \frac{R_1}{r} \ln \frac{r+R_1}{|r-R_1|} Q_{\text{syn}}(R_1, \epsilon, t) dR_1, \quad (22)$$

where $Q_{\text{syn}}(R_1, \epsilon, t)$ is the synchrotron emissivity. The function $F_{\text{KN}}(\epsilon, E_\gamma, E_e)$ is given by

$$F_{\text{KN}}(\epsilon, E_\gamma, E_e) = \frac{3\sigma_{\text{T}}}{4(E_e/m_0 c^2)^2 \epsilon} \times \left[2q \ln q + (1+2q)(1-q) + \frac{(\Gamma q)^2(1-q)}{2(1+\Gamma q)} \right] \quad (23)$$

with $\Gamma = 4\epsilon(E_e/m_0 c^2)/m_0 c^2$ and $q = E_1/\Gamma(1-E_1)$, where $E_1 = E_\gamma/E_e$ and $1/[4(E_e/m_0 c^2)] < q < 1$.

Therefore, the photon flux dN/dE_γ with energy E_γ at a radial distance r and at a time t per unit volume can be expressed as

$$E_\gamma \frac{dN(r, E_\gamma, t)}{dE_\gamma} = \frac{1}{4\pi d^2} Q_{\text{tot}}(r, E_\gamma, t), \quad (24)$$

where $Q_{\text{tot}}(r, E_\gamma, t) = Q_{\text{syn}}(r, E_\gamma, t) + Q_{\text{Comp,j}}(r, E_\gamma, t)$ and d is the distance to a source. Then the total photon flux dN/dE_γ with energy E_γ at a time t is given by

$$E_\gamma \frac{dN(E_\gamma, t)}{dE_\gamma} = \frac{1}{4\pi d^2} \int_{r_0}^{r_1} 4\pi r^2 Q_{\text{tot}}(r, E_\gamma, t) dr. \quad (25)$$

Here, we will use the following seed photon fields in the calculation of the emissivity for inverse Compton scattering: the 2.7 K CMB radiation with energy density $U_{\text{CMB}} = 0.25 \text{ eV cm}^{-3}$, the excess FIR radiation with energy density $U_{\text{FIR}} = 0.5 \text{ eV cm}^{-3}$ and temperature 46 K, starlight with energy density $U_{\text{star}} = 1.0 \text{ eV cm}^{-3}$ and temperature 5000 K, and the synchrotron radiation in the nebula.

4 RESULTS

We now give our calculation results. We will use the Crab pulsar parameters to describe the electron injection rate, i.e., the parameters in Equations (1) – (3) are as follows: $\alpha_1 = 1.4$, $\alpha_2 = 2.5$, $E_b = 1.0 \times 10^5 \text{ MeV}$, $E_{\text{max}} = 2.6 \times 10^9 \text{ MeV}$, $L_0 = 3.0 \times 10^{39} \text{ erg s}^{-1}$, $P_0 = 0.019 \text{ s}$, $I = 10^{45} \text{ g cm}^2$ and $n = 2.5$. According to VM13, on the other hand, other parameters in our calculation are $t_0 = 50$, $V_0 = 0.3$, $V_{\text{pwn}} c = 2000 \text{ km s}^{-1}$; moreover the initial size of the system is $r_s = 1.0 \text{ pc}$, initial value of β is 0.83, and the inner and outer boundaries are at $r'_0 = 0.01$ and $r'_1 = 1$ respectively. Note that different values of r'_0 will produce slightly different results. For a given distance, the decrease of r'_0 causes the decreases of the convection velocity and the magnetic field strength, but leads to the increase of the diffusion coefficient (see Eqs. (7) – (9)). Then it results in slightly different cut-off energies and magnitudes of the electron distribution. However, these differences do not affect our conclusions. Here for simplicity, we use the same value $r'_0 = 0.01$ as that of VM13.

As an example, we show the numerical results for the distributions of electrons at different radial distances r' in Figure 1. Here the magnetic field strength $B_0 = 400 \mu\text{G}$ and diffusion coefficient $\kappa_0 = 10^{-5}$ at the inner boundary, the nebula's age $t = T_{\text{age}} = 1000 \text{ yr}$, and the distance to the source $d = 2 \text{ kpc}$ are assumed. We can see that both cut-off energy E_{cut} and magnitude of electron distribution become small with the increase of the distance from $r' = 0.1$ to $r' = 0.9$. The cut-off energy is defined as the energy where the second break appears in the electron spectrum, and the electron spectrum is in units of unit volume (cubic parsec) and unit energy (MeV). At high energy, the cut-off energy is determined by the synchrotron loss and diffusion coefficient, and the particle spectra become softer as the radial distance increases which are in agreement with the results obtained by Mangano et al.

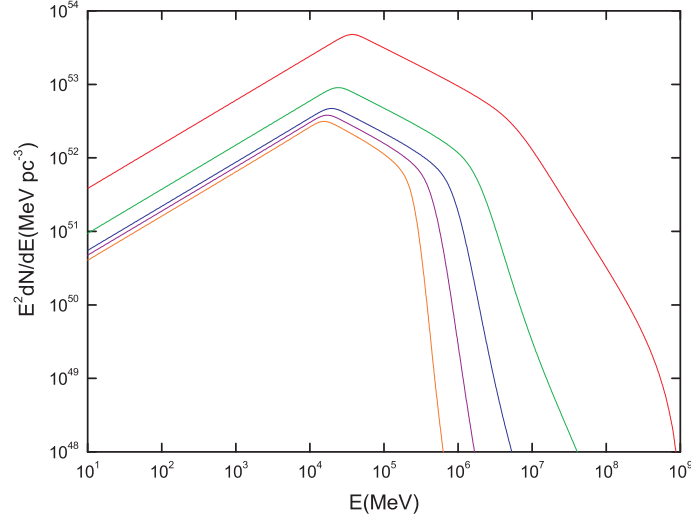


Fig. 1 Calculated electron spectra at different radial distances of $r' = 0.1$ (red line), $r' = 0.3$ (green line), $r' = 0.5$ (blue line), $r' = 0.7$ (purple line) and $r' = 0.9$ (orange line) for a PWN with an age of 1000 yr. For the parameters used see the text. Note that dN/dE represents the number of particles per unit volume (cubic parsec) in the energy interval E to $E + dE$.

(2005). Note that the projection effects on the photon emission are not considered here. The magnitude of electron distribution is determined by the convection velocity and the adiabatic loss (VM13). Using the same parameters and Equation (25), we show the calculation results for non-thermal emission in Figure 2.

Below, we study the effects of magnetic field, PWN age, maximum energy of electrons and diffusion coefficient on the evolution of particles and non-thermal photon spectra of a PWN.

4.1 The Effects of Magnetic Field, PWN Age and Maximum Energy of Electrons

At first, we consider the effect of the magnetic field on electron and non-thermal photon spectra of a PWN. In Figure 3, we show the variations of the electron spectra at $r' = 0.1$ and $r' = 0.9$ and the non-thermal photon spectra for different initial magnetic field strengths of $B_0 = 400$, 100 and 20 μG , where the PWN age $T_{\text{age}} = 1000$ yr and $\kappa_0 = 10^{-5}$ are assumed. Since the synchrotron loss rate is proportional to B^2 , the electron spectrum above E_{cut} steepens when the magnetic field strength B_0 increases. At $T_{\text{age}} = 1000$ yr, $\beta = 0.68$, so $B \approx 0.4B_0$ at $r' = 0.1$ and $B \approx 0.2B_0$ at $r' = 0.9$ from Equation (8). In this case the synchrotron loss rate decreases with the increase of radial distance. However, from Equation (9), the diffusion coefficient increases from $\kappa \approx 2.5\kappa_0 E$ to $5.1\kappa_0 E$ when the radial distance increases from $r' = 0.1$ to $r' = 0.9$, leading to a larger effect of diffusion on the electron spectrum at a larger distance. In addition, convection velocity decreases with an increase of the radial distance. Therefore, the diffusion has an important role on the steepness of the electron spectrum at a larger radial distance (see the left panel of Fig. 3). As shown in the right panel of Figure 3, because

the synchrotron radiation emissivity is proportional to B , the synchrotron radiation flux becomes higher when the magnetic field strength increases, but the inverse Compton radiation flux becomes lower with the increase of the magnetic field.

Next, we consider the effect of the PWN age on electron and non-thermal photon spectra of a PWN. We assume that $B_0 = 400 \mu\text{G}$ and $\kappa_0 = 10^{-5}$, and then calculate the electron spectra at $r' = 0.1$ and $r' = 0.9$ and non-thermal spectra for different PWN ages of $T_{\text{age}} = 1000$, 2000, 4000 and 10 000 yr. The electron spectra at $r' = 0.1$ and $r' = 0.9$ and the total electron spectra calculated by using Equation (12) are shown in Figure 4. As mentioned in Section 2.1, β is time-dependent and $\beta = 0.68$, 0.62, 0.56 and 0.50 for $T_{\text{age}} = 1000$, 2000, 4000 and 10 000 yr respectively. For $V_{\text{pwn}}c = 2000 \text{ km s}^{-1}$, the size of the system is increased by a factor of 2.7, 5.4, 10.2 and 21.1 relative to the original size for $T_{\text{age}} = 1000$, 2000, 4000 and 10 000 yr, respectively. Both the changes of β and the size of the system would lead to variations in the magnetic field strength, in the convection velocity and in the diffusion coefficient (see Eqs. (7) – (9)).

At $r' = 0.1$, the values of the magnetic field strength, the convection velocity, and the diffusion coefficient are $B/B_0 = 0.40, 0.24, 0.14$ and 0.07 , $V/V_0 = 0.15, 0.095, 0.08$ and 0.071 and $\kappa/\kappa_0 E = 2.48, 4.22, 7.30$ and 14.08 for $T_{\text{age}} = 1000, 2000, 4000$ and $10 000$ yr, respectively. At $r' = 0.9$, corresponding values are $B/B_0 = 0.19, 0.10, 0.05$ and 0.02 , $V/V_0 = 0.032, 0.024, 0.023$ and 0.022 , and $\kappa/\kappa_0 E = 5.11, 9.72, 19.19$ and 42.53 , respectively. These variations lead to decreases of synchrotron loss and the convection effect but an increase of the effect of diffusion at a larger radial distance with the increase of the PWN age. On the other hand, because of the system's expansion (which leads to a larger adiabatic loss in the inner part of

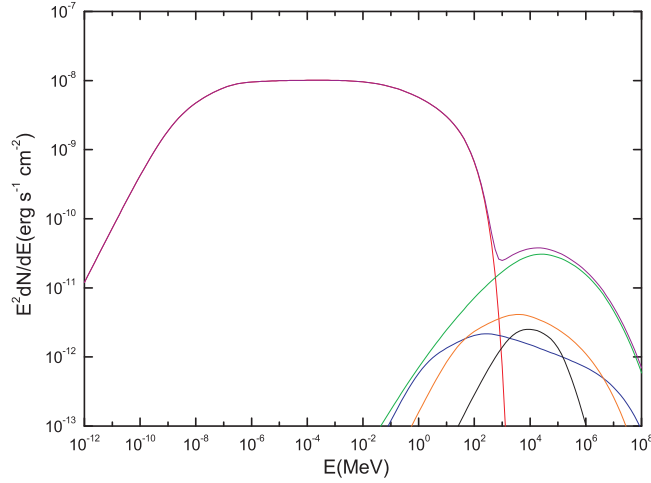


Fig. 2 Calculated non-thermal photon spectra for a PWN with an age of 1000 yr. The spectra of synchrotron radiation (*red line*), inverse Compton scattering off the synchrotron photons (*green line*), CMB (*blue line*), IR (*orange line*) and starlight (*black line*), and the total emission (*purple line*) are shown. The parameters used are the same as those in Fig. 1.

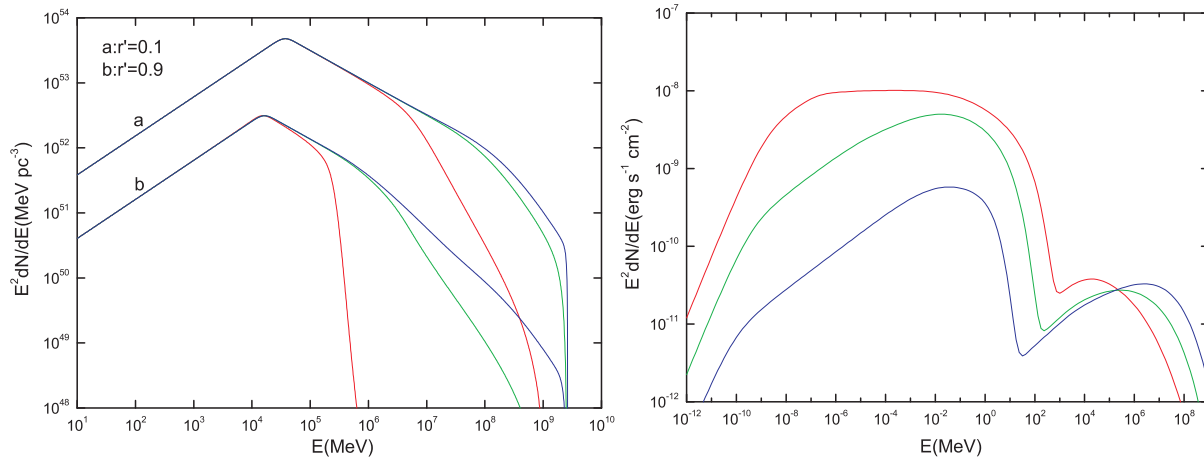


Fig. 3 *Left panel*: Calculated electron spectra at $r' = 0.1$ and $r' = 0.9$ for different initial magnetic field strengths of $B_0 = 400 \mu\text{G}$ (*red line*), $100 \mu\text{G}$ (*green line*) and $20 \mu\text{G}$ (*blue line*). The values of $T_{\text{age}} = 1000 \text{ yr}$ and $\kappa_0 = 10^{-5}$ are assumed. *Right panel*: Corresponding non-thermal photon spectra calculated by Eq. (25).

the system) and the decreases of the spin-down power $L(t)$ (which results in the decrease of electron injection rate) with the increase of the PWN age, the electron energy density becomes lower and is dominated at $E \gtrsim 1 \text{ TeV}$ by the diffusion and synchrotron loss when the PWN age increases. Moreover, the electrons will travel further through the system as time increases, which leads to more synchrotron loss and then makes the electron spectrum steep. Compared to the electron spectra at $r' = 0.1$, the spectra at $r' = 0.9$ become harder with time, which are the same as those in VM13. The reason is mainly that the synchrotron loss decreases quickly with time and becomes less important in the outer parts of the system. Note that the total electron spectra at different PWN ages only show small differences, i.e., the maximum energy of the particles will exhibit a slight decrease with time, and the total number density of electrons will display a slight increase with time

(see the bottom panel of Fig. 4). These results are in agreement with those obtained by Zhang et al. (2008). For the maximum energy of particles, a slight decrease with time is consistent with the result given by Torres et al. (2014). The corresponding non-thermal photon spectra calculated by using Equation (25) are shown in Figure 5. Since β decreases with time, the synchrotron radiation will decrease with time. Therefore, non-thermal photon spectra at different PWN ages have significant differences.

Finally, we study the effect of the maximum energy of electrons on electron and non-thermal photon spectra of a PWN. In Figure 6, we show the variations of the electron spectra at $r' = 0.1$ and $r' = 0.9$ and the non-thermal photon spectra for different maximum energies of $E_{\text{max}} = 1.0 \times 10^{10}$, 1.0×10^9 , 1.0×10^8 and $1.0 \times 10^7 \text{ MeV}$, where $T_{\text{age}} = 1000 \text{ yr}$, $B = 400 \mu\text{G}$ and $\kappa = 10^{-5}$ are used. Since the diffusion coefficient is proportional

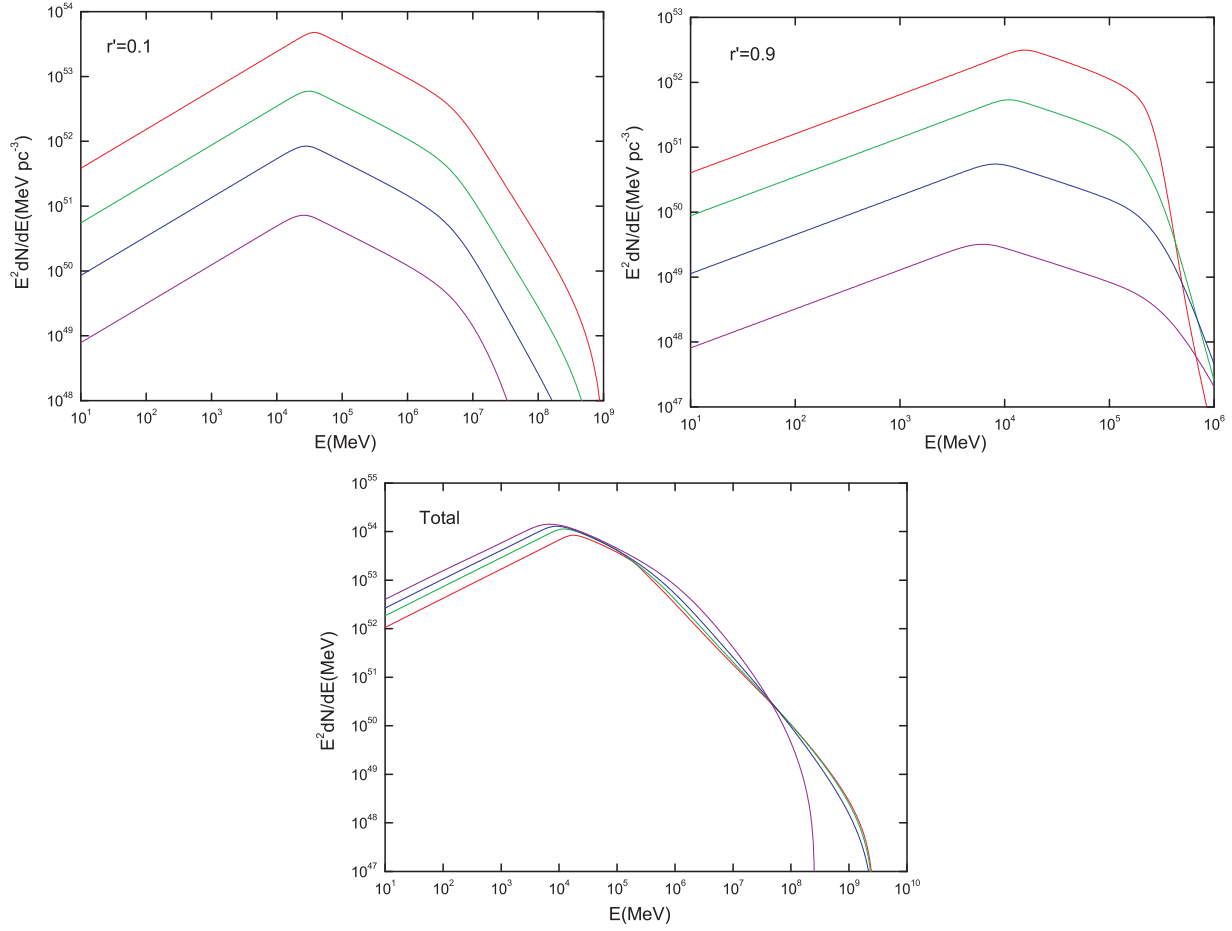


Fig. 4 Calculated electron spectra at different radii of $r' = 0.1$ and $r' = 0.9$ in the expanding system and the total electron spectra for different ages of $T_{\text{age}} = 1000$ yr (red line), 2000 yr (green line), 4000 yr (blue line) and 10 000 yr (purple line). Top left panel: the spectra at $r' = 0.1$. Top right panel: the spectra at $r' = 0.9$. Bottom panel: the total electron spectra.

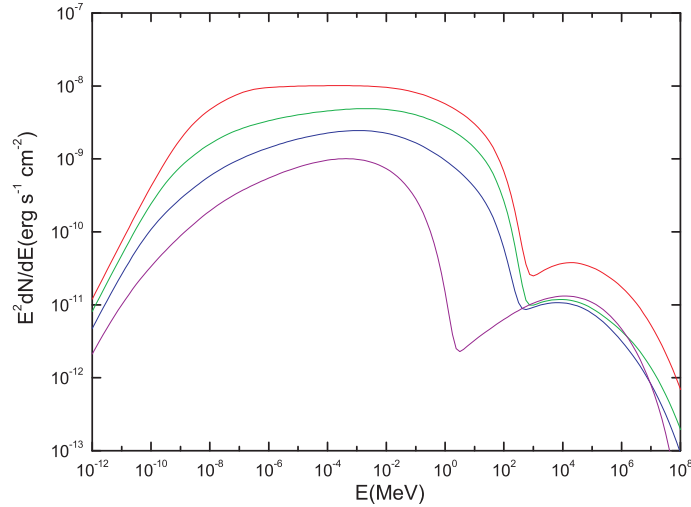


Fig. 5 Calculated non-thermal photon spectra at $T_{\text{age}} = 1000$ yr (red line), 2000 yr (green line), 4000 yr (blue line) and 10 000 yr (purple line). The parameters used are the same as those in Fig. 4.

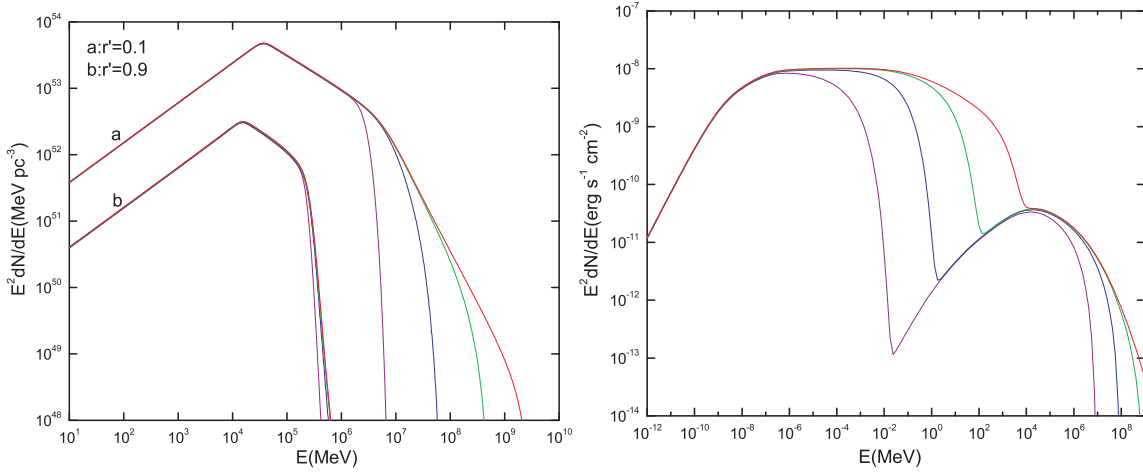


Fig. 6 Calculated electron spectra (*left panel*) at $r' = 0.1$ and $r' = 0.9$ and the corresponding non-thermal photon spectra (*right panel*) for different maximum energies of $E_{\max} = 1.0 \times 10^{10}$ MeV (*red line*), 1.0×10^9 MeV (*green line*), 1.0×10^8 MeV (*blue line*) and 1.0×10^7 MeV (*purple line*). The other parameters used are the same as those in Fig. 1.

to E and the free-escape boundary is $f(r', E_{\max}) = 0$, the electron spectra above E_{cut} steepen when the maximum energy decreases. Compared to the electron spectra at $r' = 0.1$, the spectra at $r' = 0.9$ do not show a significant change. This is because the higher energy particles lose more energy when the particles travel further through the system, which leads to the magnitude of the distribution of higher energy particles being small. The calculated results for the corresponding non-thermal photon emission are shown in the right panel of Figure 6. Since the electron spectra vary with the maximum energy of electrons, the non-thermal photon spectra at different E_{\max} have significant differences.

4.2 The Effect of Diffusion

To study the effect of diffusion on the electron spectrum in a PWN, we first consider variations of the diffusion timescale τ_{diff} , convection timescale τ_{con} , synchrotron cooling timescale τ_{syn} , inverse Compton cooling timescale τ_{IC} and adiabatic loss timescale τ_{ad} with electron energy at different radial distances for different values of κ_0 .

In Figure 7, we show the variations of the above five timescales with electron energy at $r' = 0.1$ and $r' = 0.9$ for $\kappa_0 = 1.0 \times 10^{-2}$, 1.0×10^{-3} , 1.0×10^{-4} and 1.0×10^{-5} , where $B_0 = 400 \mu\text{G}$ and $T_{\text{age}} = 1000$ yr are used. Since τ_{con} and τ_{ad} are energy-independent but τ_{diff} and τ_{syn} are energy-dependent (both $\propto 1/E$), we can introduce a dimensionless parameter to account for the competition between the synchrotron loss and effect of diffusion: $\xi = \tau_{\text{diff}}/\tau_{\text{syn}} \propto (B_0^2/\kappa_0)(r/r_0)^{3\beta-1}$ (see Eqs. (13) and (15)). Therefore, there are three regimes for the competition between the synchrotron loss and the effect of diffusion: $\xi \ll 1$ represents the diffusion dominated regime, $\xi \sim 1$ the synchrotron/diffusion dominated regime and $\xi \gg 1$ the synchrotron dominated regime.

In Figure 7, the propagation effects of the electron spectrum at $r' = 0.1$ are dominated by convection (at lower energy) and synchrotron loss (at higher energy) when $\kappa_0 > 10^{-4}$, otherwise this process is dominated by convection (at lower energy) and diffusion (at higher energy) (see the left panel of Fig. 7); but at $r' = 0.9$, the value of κ_0 becomes about 10^{-3} (see the right panel of Fig. 7).

We now turn to calculate the electron spectra and non-thermal photon spectra for different diffusion coefficients of $\kappa_0 = 1.0 \times 10^{-2}$, 1.0×10^{-3} , 1.0×10^{-4} , 1.0×10^{-5} and 0.0, where $B_0 = 400 \mu\text{G}$ and $T_{\text{age}} = 1000$ yr are used. The results are shown in Figure 8. For the electron spectra (see the left panel of Fig. 8), we consider the case of $\kappa_0 = 0$ (i.e. $\tau_{\text{diff}} \rightarrow \infty$). As mentioned above, the propagation effects of the electron spectrum are dominated by convection (at lower energy) and synchrotron loss (at higher energy) (see Fig. 7). At $r' = 0.1$, the propagation effects of the electron spectrum at the high energy regime are dominated by synchrotron loss for $\kappa_0 = 10^{-5}$ (i.e., $\xi \gg 1$), diffusion and synchrotron loss when $\kappa_0 = 10^{-4}$ (i.e., $\xi \sim 1$), and diffusion $\kappa_0 = 10^{-2}$ (i.e., $\xi \ll 1$), leading to different changes of spectral shape at the high energy regime. At a larger radial distance (say $r' = 0.9$), the value of ξ at $r' = 0.9$ increases by a factor of about 10 relative to that at $r' = 0.1$, so the division into three regimes mentioned above also changes and then the corresponding spectral shapes are different from those at $r' = 0.1$ (see the left panel of Fig. 7). In the right panel of Figure 8, we show the corresponding non-thermal photon spectra, which indicate that the effect of diffusion has an important role on the spectral shape of electrons at the high energy regime.

Finally, we investigate the effect of diffusion on electron spectra and non-thermal photon spectra in different PWN ages. In order to do so, we consider two cases with diffusion (assuming $\kappa_0 = 10^{-5}$) and without diffusion ($\kappa_0 = 0$) at the PWN ages of $T_{\text{age}} = 1000, 2000, 4000$

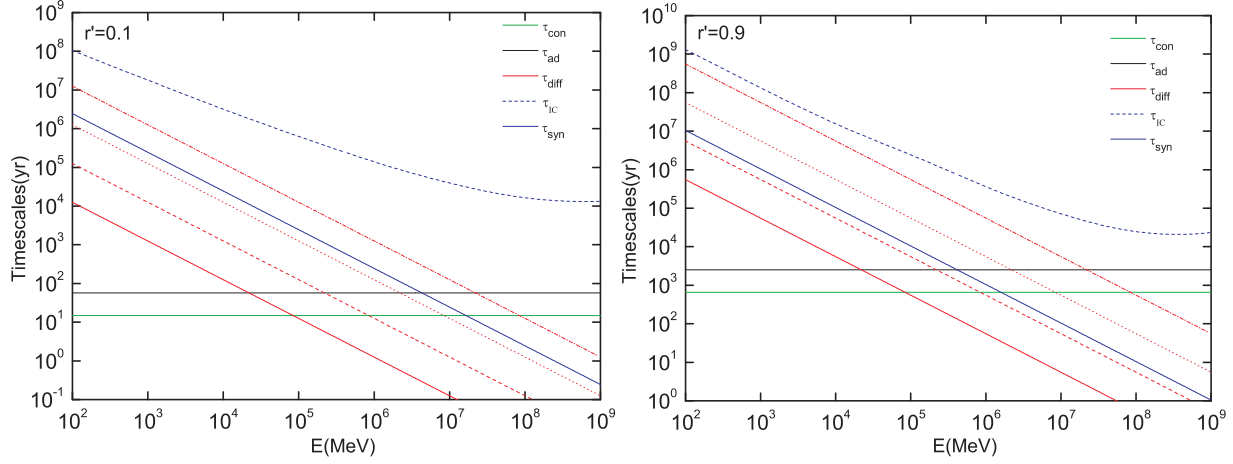


Fig. 7 Changes of τ_{diff} , τ_{con} , τ_{IC} , τ_{syn} and τ_{ad} at $r' = 0.1$ and $r' = 0.9$ with electron energy for different initial diffusion coefficients of $\kappa_0 = 1.0 \times 10^{-2}$ (red solid line), 1.0×10^{-3} (red dashed line), 1.0×10^{-4} (red dotted line) and 1.0×10^{-5} (red dash-dotted line). $B_0 = 400 \mu\text{G}$ and $T_{\text{age}} = 1000 \text{ yr}$ are used.

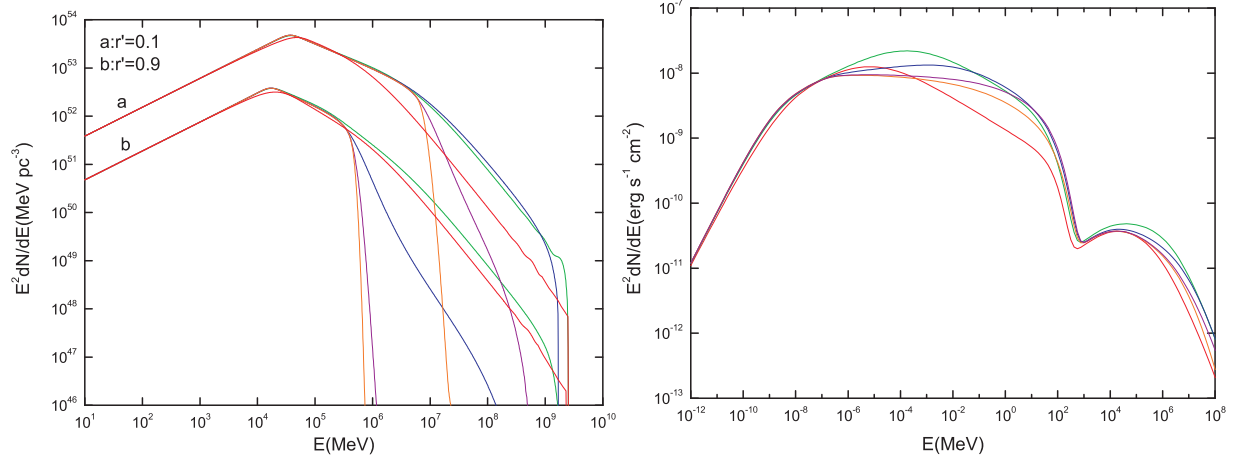


Fig. 8 Calculated electron spectra (left panel) at $r' = 0.1$ and $r' = 0.9$ and non-thermal photon spectra (right panel) for different diffusion coefficients of $\kappa_0 = 1.0 \times 10^{-2}$ (red line), 1.0×10^{-3} (green line), 1.0×10^{-4} (blue line), 1.0×10^{-5} (purple line) and 0.0 (orange line). $B_0 = 400 \mu\text{G}$ and $T_{\text{age}} = 1000 \text{ yr}$ are used.

and 10 000 yr, where $B_0 = 400 \mu\text{G}$ is used. The results are shown in Figure 9. In the absence of diffusion, the synchrotron cut-off of the electron spectrum at the high energy end shifts to lower energy as time increase. This is because the electrons in the system have a longer residence time and will lead to more synchrotron loss. At $r' = 0.1$, there is an obvious difference of electron spectra with and without diffusion at each PWN age (see the left top panel of Fig. 9). At $r' = 0.9$, however, the spectra with and without diffusion at each PWN age just show a small difference, indicating that the effect of diffusion on the spectra at each PWN age has only a minor role when $\kappa_0 = 10^{-5}$ is used, which is consistent with the result of VM13. Of course, this result depends on the initial diffusion coefficient used (here, $\kappa_0 = 10^{-5}$). As mentioned above, if a larger value of κ_0 is applied, then the effect of diffusion on

the spectra at each PWN age has an important role to change the particle spectral index even at $r' = 0.9$ (see Fig. 8). Tang & Chevalier (2012) used the models with diffusion of particles to fit the spectral index profiles of Crab, 3C58 and G21.5-0.9. Their results implied that the models with particle diffusion are much better for fitting spectral index profiles than pure advection models, which means that diffusion is important for changing the particle spectral index.

5 SUMMARY AND DISCUSSION

In this paper, assuming a time-dependent broken power-law injection and numerically solving the Fokker-Planck transport equation including convection, diffusion, adiabatic loss and radiative loss in spherical coordinates, we have studied the spatial dependence of high energy electrons and their radiations in a PWN. In this model with

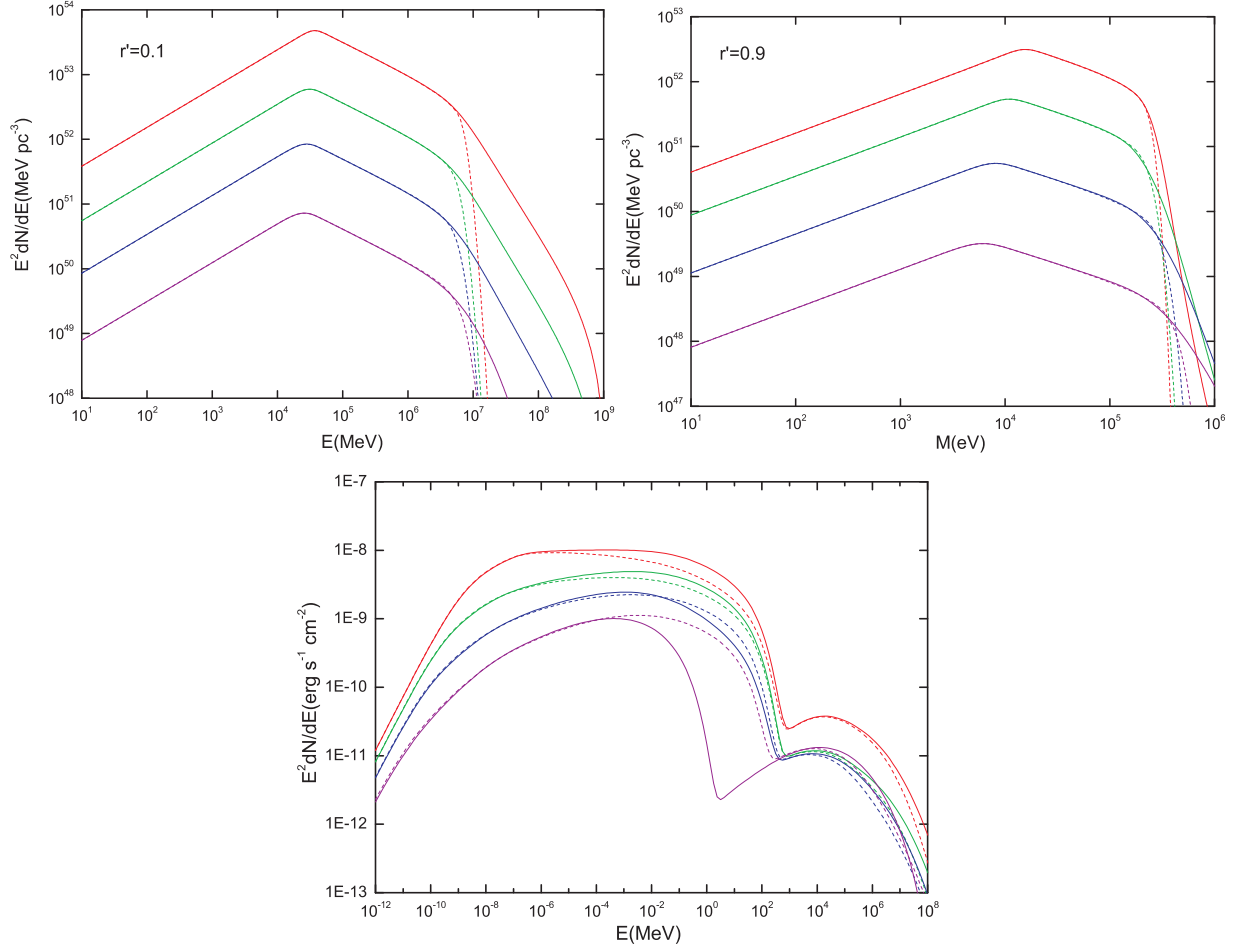


Fig. 9 Calculated electron spectra at $r' = 0.1$ (top left panel) and $r' = 0.9$ (top right panel) and non-thermal photon spectra (bottom panel) in the cases with $\kappa_0 = 10^{-5}$ (solid lines) and $\kappa_0 = 0$ (dashed lines) at different PWN ages of $T_{\text{age}} = 1000$ yr (red line), 2000 yr (green line), 4000 yr (blue line) and 10 000 yr (purple line). $B_0 = 400 \mu\text{G}$ is used.

the expansion of the system, the effects of magnetic field, PWN age, maximum energy of electrons, and diffusion on electron spectra and their radiations are studied in detail.

In our calculations, the parameters of the Crab pulsar are used to describe the electron injection rate and the expansion velocity of constant $V_{\text{pwn}}c = 2000 \text{ km s}^{-1}$ is assumed. In this case, the convection velocity, adiabatic loss, magnetic field strength, and diffusion coefficient are spatially-dependent. Therefore, the electron spectra at different radial distances are totally different, indicating the maximum energy of the electron spectrum decreases with the increase of radial distance (see Fig. 1). Because of the competition between synchrotron loss (which is proportional to B^2) and the particle diffusion in the high energy region, different magnetic field strengths result in variations of the electron spectra at high energy parts, and then the synchrotron radiation flux becomes higher, but the inverse Compton radiation flux becomes lower with the increase of the magnetic field (see Fig. 3). Note that it has been shown that a constant expansion velocity is reasonable only when the age of the PWN is younger than 10 kyr (Gelfand et al. 2009). Therefore, we have calculated

the electron spectra at different radial distances and non-thermal photon spectra for different PWN ages. Since the system expands and the index β decreases with time, the magnetic field strength decreases but the diffusion coefficient increases as the PWN age increases, leading to significantly different particle spectra at different PWN ages (see Fig. 4). The results indicate that the electron energy density becomes lower when the PWN age increases and is dominated at $E \gtrsim 1 \text{ TeV}$ by the diffusion and the synchrotron loss. We also studied the effect of the maximum energy of electrons on electron spectra and corresponding non-thermal photon spectra in a fixed PWN age (see Fig. 6), and found that the maximum energy of electrons is important for changing the particle spectral index at the high energy regime.

Our results indicated that particle diffusion is important for the evolution of particle spectra, especially in the higher energy region. For a fixed PWN age and a given B_0 , the effect of diffusion can be divided into three regimes: $\xi \ll 1$, the cut-off energy of the particle spectrum in the high energy end is dominated by the particle diffusion; $\xi \sim 1$, the particle spectrum is dominated by the processes

of synchrotron loss and particle diffusion; and $\xi \gg 1$, the particle diffusion is not important. Note that such a division depends on the radial distance (see Fig. 7). We have shown that different diffusion coefficients lead to different electron spectra and non-thermal photon spectra (see Fig. 8). Moreover, the electron spectra and the non-thermal photon spectra with ($\kappa_0 = 10^{-5}$) and without diffusion ($\kappa_0 = 0$) are different for various PWN ages. Particle diffusion is important for reducing the synchrotron loss when $T_{\text{age}} \lesssim 4000$ yr (see Fig. 9). As time increases, the particle diffusion increases rapidly, so the particles travel further through the system and experience more synchrotron loss. Therefore, the cut-off of the electron spectrum at the high energy end becomes lower, which has traditionally been attributed to the synchrotron loss alone (Schöck et al. 2010). Here due to the competition between diffusion and synchrotron loss, the effect of diffusion is important for

changing the particle spectral index and similar results are shown in Tang & Chevalier (2012). Therefore we conclude that the higher energy part of the electron spectrum is dominated by the competition between synchrotron loss and diffusion, and the effect of diffusion has an important role on the evolution of electron spectra as well as non-thermal photon spectra in a PWN.

Acknowledgements This work is partially supported by the National Natural Science Foundation of China (Grant Nos. 11433004 and 11173020), the Top Talents Program of Yunnan Province, the Natural Science Foundation of Yunnan Province (2012FD055 and 2013FB063), the Young Teachers Program of Yuxi Normal University, and the Program for Innovative Research Team (in Science and Technology) in University of Yunnan Province (IRTSTYN).

Appendix A: THE NUMERICAL METHOD FOR THE TRANSPORT EQUATION

In order to discretize the transport equation, we define

$$f_{j,k}^i = f(r'_j, E_k, i\Delta t), \quad (\text{A.1})$$

$$\delta_{r'}^2 f_{jk}^i = \frac{f_{j+1k}^i - 2f_{jk}^i + f_{j-1k}^i}{\Delta r'^2}, \quad (\text{A.2})$$

$$\delta_{r'} f_{jk}^i = \frac{f_{j+1k}^i - f_{j-1k}^i}{2\Delta r'}, \quad \delta_E f_{jk}^i = \frac{f_{jk+1}^i - f_{jk-1}^i}{2\Delta \ln E}. \quad (\text{A.3})$$

Equation (5) can be rewritten as

$$\begin{aligned} \frac{f_{j,k}^{i+\frac{1}{2}} - f_{j,k}^i}{\Delta t} &= \frac{1}{2} \left[S_1^{i+\frac{1}{2}} \delta_{r'}^2 \left(f_{jk}^{i+\frac{1}{2}} + f_{jk}^i \right) + S_2^{i+\frac{1}{2}} \delta_{r'} \left(f_{jk}^{i+\frac{1}{2}} + f_{jk}^i \right) \right] \\ &\quad + S_3^i \delta_E f_{jk}^i + 4z_j^{i+\frac{1}{2}} E_k f_{jk}^{i+\frac{1}{2}}, \end{aligned} \quad (\text{A.4})$$

$$\frac{f_{j,k}^{i+1} - f_{j,k}^{i+\frac{1}{2}}}{\Delta t} = \frac{1}{2} S_3^{i+1} \left[\delta_E \left(f_{jk}^{i+1} - f_{jk}^i \right) \right], \quad (\text{A.5})$$

where the S coefficients are

$$S_1^i = \frac{\kappa_{jk}^i}{\rho_i^2}, \quad (\text{A.6})$$

$$S_2^i = \frac{1}{\rho_i} \left[\frac{2\kappa_{jk}^i}{\rho_i r'_j + \varepsilon_i} + \frac{1}{\rho_i} \frac{\kappa_{j+1k}^i - \kappa_{j-1k}^i}{2\Delta r'} + V_{\text{pwn}} \frac{r'_j - r'_0}{r'_{\text{max}} - r'_0} - V_j^i \right], \quad (\text{A.7})$$

$$S_3^i = \left[\frac{2V_j^i}{3(\rho_i r'_j + \varepsilon_i)} + \frac{1}{3\rho_i} \frac{V_{j+1}^i - V_{j-1}^i}{2\Delta r'} + z_j^i E_k \right], \quad (\text{A.8})$$

and

$$S_1^{i+\frac{1}{2}} = \frac{S_1^i + S_1^{i+1}}{2}, \quad S_2^{i+\frac{1}{2}} = \frac{S_2^i + S_2^{i+1}}{2}, \quad z_j^{i+\frac{1}{2}} = \frac{z_j^i + z_j^{i+1}}{2}. \quad (\text{A.9})$$

Equation (A.4) and Equation (A.5) can be translated into tridiagonal equations and are then solved numerically (Press et al. 1989).

References

- Atoyan, A. M., & Aharonian, F. A. 1996, MNRAS, 278, 525
- Blumenthal, G. R., & Gould, R. J. 1970, *Reviews of Modern Physics*, 42, 237
- Douglas, J. 1962, *Numerische Mathematik*, 4, 41
- Fang, J., & Zhang, L. 2010, ApJ, 718, 467
- Gaensler, B. M., & Slane, P. O. 2006, ARA&A, 44, 17
- Gelfand, J. D., Slane, P. O., & Zhang, W. 2009, ApJ, 703, 2051
- Kargaltsev, O., Rangelov, B., & Pavlov, G. G. 2014, American Astronomical Society, AAS Meeting 223, 153.22, arXiv:1305.2552
- Kennel, C. F., & Coroniti, F. V. 1984, ApJ, 283, 694
- Li, H., Chen, Y., & Zhang, L. 2010, MNRAS, 408, L80
- Mangano, V., Massaro, E., Bocchino, F., Mineo, T., & Cusumano, G. 2005, A&A, 436, 917
- Martín, J., Torres, D. F., & Rea, N. 2012, MNRAS, 427, 415
- Moderski, R., Sikora, M., Coppi, P. S., & Aharonian, F. 2005, MNRAS, 363, 954
- Parker, E. N. 1965, *Planet. Space Sci.*, 13, 9
- Press, W. H., Flannery, B. P., Teukolsky, S. A., & Vetterling, W. T. 1989, *Numerical Recipes in Pascal. The Art of Scientific Computing* (Cambridge: Cambridge University Press)
- Rees, M. J., & Gunn, J. E. 1974, MNRAS, 167, 1
- Rybicki, G. B., & Lightman, A. P. 1979, *Radiative Processes in Astrophysics* (New York: Wiley-Interscience)
- Schöck, F. M., Büsching, I., de Jager, O. C., Eger, P., & Vorster, M. J. 2010, A&A, 515, A109
- Tanaka, S. J., & Takahara, F. 2010, ApJ, 715, 1248
- Tang, X., & Chevalier, R. A. 2012, ApJ, 752, 83
- Torres, D. F., Cillis, A., Martín, J., & de Oña Wilhelmi, E. 2014, *Journal of High Energy Astrophysics*, 1, 31
- Venter, C., & de Jager, O. C. 2006, in *Proc. 363rd WE-Heraeus Seminar on Neutron Stars and Pulsars*, ed. W. Becker & H.-H. Huang (MPERep. 291; Garching: MPI Extraterr. Phys.), 40, <http://adsabs.harvard.edu/abs/2007whsn.conf.....B>
- Vorster, M. J., & Moraal, H. 2013, ApJ, 765, 30
- Vorster, M. J., Tibolla, O., Ferreira, S. E. S., & Kaufmann, S. 2013, ApJ, 773, 139
- Weiler, K. W., & Panagia, N. 1978, A&A, 70, 419
- Zhang, L., & Fang, J. 2007, ApJ, 666, 247
- Zhang, L., Chen, S. B., & Fang, J. 2008, ApJ, 676, 1210
- Zhu, B.-T., Fang, J., & Zhang, L. 2015, MNRAS, 451, 3145